AN EFFICIENT METHOD FOR TEXTURE DEFECT DETECTION: SUBBAND DOMAIN CO-OCCURRENCE MATRICES

Ahmet Latif Amet[1], *Ayşın Ertüzün*[1], *Aytül Erçil* [2]

[1]Department of Electrical-Electronics Engineering
[2]Department of Industrial Engineering
Boğaziçi University
Bebek 80815, Istanbul, TURKEY.
latif@busim.ee.boun.edu.tr, ertuz@boun.edu.tr, ercil@boun.edu.tr

Phone: (+90)-212-2631540/1852 (secr. 1414)
Fax: (+90)-212-2872465

ABSTRACT

In this paper, an efficient algorithm, which combines concepts from wavelet theory and co-occurrence matrices, is presented for detection of defects encountered in textile images. Detection of defects within the inspected texture is performed first by decomposing the gray level images into sub-bands, then by partitioning the textured image into non-overlapping sub-windows and extracting the co-occurrence features and finally by classifying each sub-window as defective or non-defective with a Mahalanobis distance classifier being trained on defect free samples a priori. The experimental results demonstrating the use of this algorithm for the visual inspection of textile products obtained from the real factory environment are also presented. Experiments show that focusing on a particular band with high discriminatory power improves the detection performance as well as increases the computational efficiency.

Key words: Texture Defect Detection

Co-occurrence Matrices

Wavelet filters

1. Introduction

Visual inspection constitutes an important part of quality control in industry. Quality control is designed to ensure that defective products are not allowed to reach the customer. For this reason, quality control activities form an essential information feedback loop for the whole business, with potential influence on the design, process planning and logistics functions as well as on manufacturing. Until recent years, this job has been heavily relied upon human inspectors. Development of fast and specialized equipment, however, has facilitated the application of image processing algorithms to real-world industrial inspection problems.

Texture analysis has nearly three decades long past. During the seventies and early eighties, the algorithms have been mainly based on first and second order statistics of the image pixel gray level values as spatial domain gray level co-occurrence matrix (SDCM) and neighboring gray level dependence matrix (NGLDM) [1-3]. In mid-eighties, model based methods such as Markov Random Fields (MRF) and simultaneous autoregressive (SAR) models have appeared as an alternative. Wavelets, although have been known for many years, received the attention of image processing society only after the papers of Daubechies [4], who has provided the discretization of the wavelet transform (WT), and Mallat [5], who has established the connection between the WT and the multi-resolution theory. Thus, starting from the late eighties, signal processing methods based on Gabor transform and the WT have replaced the statistical and model based methods [6-8]. Representing signals in multiple resolutions by the WT is believed to enable extraction of more powerful features than the single scale case. Features extracted are, mainly, based on band energy and entropy. Although frequency based features work well for most of the applications, it can not be argued that this will be true for all of the cases as shown in [3] and [9], where statistical features outperformed the former.

One of the application areas of texture analysis is defect detection in textured images. Texture defect detection can be defined as the process of determining the location and/or extend of a collection of pixels in a textured image with remarkable deviation in their intensity values or spatial arrangement with respect to the background texture.

Most of the texture defect detection applications are on textile, paper, steel and wood inspection. There have been a number of applications of texture processing to inspection problems. Erçil *et.al.* [10] have proposed a model-based technique to detect and locate the various kinds of defects that might be present in a given painted surface. Jain *et.al.* [11] have used the texture features computed from a bank of Gabor filters to automatically classify the uniformity of painted metallic surfaces. Chen and Jain *et.al*. [12] have used a structural approach to defect detection in textured images. Conners *et.al*. [13] have utilized texture analysis methods to detect defects in lumber wood automatically. Siew *et.al.* [2] have proposed a method for the assessment of carpet wear. Dewaele *et.al.* [14] have used signal processing methods to detect point and line defects in texture images. Cohen *et.al.* [15] have modeled textile fabric images through MRF and used easily computable sufficient statistics as features in place of model parameters during the classification of samples as defective or non-defective via a generalized likelihood test. Lee *et.al.* [16] have used neural networks to classify defects through energy and entropy features computed from the adaptive wavelet packet expansion of the steel images. Jasper *et. al.* [17] have demonstrated that the adaptive wavelet basis can be used to locate defects in woven fabrics. Song *et. al.* [18] have developed a color clustering scheme based on human color perception. This scheme together with the texture information is used to detect defects in textured images. Iamberlini *et.al.* [19] have developed an optical method that uses Fourier transformation and spatial filtering. This method is used for real time defect detection in textured images. Campbell and Muırtagh[20] have used morphological filtering to extract texture features, to detect localized and extended flaw patterns. The performance of the system is tested on denim fabric that contains real defects.

In this study, an efficient new method, namely, the sub-band domain co-occurrence matrix (SBCM) method [21] is presented. It is shown how combined use of two approaches, i.e. extracting frequency based features through signal processing methods (such as WT) and statistical features from SDCM can lead to effective solutions for the texture analysis problems particularly, the texture defect detection problem. WT is used to determine the frequency bands carrying the most information about the texture by decomposing images into multiple frequency bands and computing the band energies. This can be viewed as dimensionality reduction or removing the irrelevant data prior to the feature extraction process. Thus, WT offers the ability of robust feature extraction in images. Then Haralick features [1] are extracted from the co-occurrence matrices computed from the sub-bands that represent the texture best. In the detection part, Mahalanobis distance classifier is used to decide whether the test image is defective or not.

Organization of the paper is as follows: Section II introduces the background theory for the WT and the co-occurrence matrices. Section III describes the proposed texture defect detection system. Implementation details and experimental results are summarized in Section IV. Finally, Section V includes the concluding remarks.

2. MATHEMATICAL FRAMEWORK

2.1. Wavelet Transform

WT is defined as a decomposition of a signal with a family of real orthonormal basis functions, $\psi_{m,n}(x)$, obtained through translation and dilation of a kernel function, $\psi(x)$, known as the mother wavelet [1,4,5,8,16].

$$\psi_{m,n}(x) = 2^{-m/2}\psi(2^{-m}x - n) \tag{1}$$

where m and n are integers. Since $\psi_{m,n}(x)$ form an orthonormal set, the analysis and synthesis formula for a signal $f(x)$ are, respectively, given by

$$c_{m,n} = \int_{-\infty}^{+\infty} f(x)\psi_{m,n}(x)dx \tag{2}$$

$$f(x) = \sum_{m,n} c_{m,n} \psi_{m,n}(x) \tag{3}$$

The mother wavelet can be constructed by first determining a scaling function satisfying the two-scale difference equation

$$\phi(x) = \sqrt{2} \sum_{k} h(k) \phi(2x - k) \tag{4}$$

and then relating $\psi(x)$ to the scaling function via

$$\psi(x) = \sqrt{2} \sum_{k} g(k) \phi(2x - k) \tag{5}$$

where

$$g(k)=(-1)^k h(1-k)\,. \tag{6}$$

In order to have wavelet bases obtained through the above procedure be unique, orthonormal and have desired regularity, the coefficients $h(k)$ have to meet certain conditions[22]. Nice thing about this decomposition scheme is that one does not need to calculate explicitly the scaling and mother wavelet functions, but can obtain the transform coefficients, recursively, using $h(k)$ and $g(k)$. A J-level decomposition can be written as

$$\begin{aligned} f(x) &= \sum_{k} c_{0,k} \phi_{0,k}(x) \\ &= \sum_{k} (c_{J+1,k} \phi_{J+1,k}(k) + \sum_{j=0}^{J} d_{j+1,k} \psi_{j+1,k}(x)) \end{aligned} \tag{7}$$

where coefficients $c_{0,k}$ are given and coefficients $c_{j+1,n}$ and $d_{j+1,n}$ at scale $j+1$ are related to the coefficients $c_{j,n}$ at scale j via

$$c_{j+1,n} = \sum_{k} c_{j,k} h(k - 2n) \tag{8a}$$

$$d_{j+1,n} = \sum_{k} d_{j,k} g(k - 2n) \tag{8b}$$

for $0 \le j \le J$. In signal processing terms, operations in Eq. (8) is nothing but convolving coefficients $c_{j,n}$ and $d_{j,n}$ at resolution j with $\tilde{h}(n)$ and $\tilde{g}(n)$ and down-sampling by two (dropping every other sample) to obtain $c_{j+1,n}$ and $d_{j+1,n}$. Here $\tilde{h}(n)$ and $\tilde{g}(n)$ are defined as

$$\tilde{h}(n) = h(-n) \tag{9a}$$

$$\tilde{g}(n) = g(-n) \tag{9b}$$

and can be regarded as impulse responses of quadrature mirror lowpass and highpass filters H and G, respectively. Decomposition in the conventional wavelet transform scheme that is also called pyramid structured wavelet transform (PSWT) is carried recursively on the output of filter $\tilde{h}(n)$. The output of *J*-level decomposition will contain the low-resolution coefficient $c_{j,n}$ and detail coefficients $d_{j,n}$ for each level ($1 \le j \le J$) (Fig.1). In the synthesis, the procedure works opposite, i.e., the low-resolution coefficient $c_{J,n}$ and detail coefficients $d_{j,n}$ are first upsampled by two (inserting a zero between neighboring samples) and then filtered with $h(n)$ and $g(n)$ respectively. Decomposition in the conventional wavelet transform scheme that is also called pyramid structured wavelet transform is carried recursively on the output of filter $\tilde{h}(n)$. This, in signal processing terms, is equivalent to splitting each time the low-frequency band. This is suitable for signals with most of their energy concentrated in the low frequency regions.

Extension of wavelet to 2-D is achieved by expressing the 2-D basis functions as tensor product of two 1-D wavelet basis functions along the horizontal and vertical directions. The corresponding filter coefficients can be computed via[23]

$$h_{\mathrm{LL}}(k, l) = h(k)h(l) \tag{10a}$$

$$h_{\mathrm{LH}}(k, l) = h(k)g(l) \tag{10b}$$

$$h_{\mathrm{HL}}(k, l) = g(k)h(l) \tag{10c}$$

$$h_{\mathrm{HH}}(k, l) = g(k)g(l) \tag{10d}$$

WT, though new compared to the other orthogonal transformations such as discrete cosine transform (DCT), discrete sine transform (DST) and discrete Fourier transform (DFT), has become very popular and has been used in a wide range of image processing applications, ranging from segmentation to classification problems and from compression to detection algorithms. The wavelet transform of an image generates a data structure known as scale-space representation. In

this representation, spatial/spatial-frequency resolution is not fixed as in DCT, DST and DFT, but change in an optimal way. Namely, the spatial resolution increases with frequency, and spatial-frequency resolution becomes narrower as frequency decreases. So high frequency signals are precisely located in spatial domain, while the low-frequency signals are precisely located in the frequency domain. Sharp edges, which are well localized spatially and have a significant high frequency content, can be represented more compactly by WT than the other transforms. Furthermore, WT is computationally attractive, and does not introduce redundancy. An image can be represented in multiple resolutions by the same amount of data with the original form (Fig. 2).

2.2. Co-occurrence Matrices

Among all statistical methods, the most popular one which is based on the estimation of the second order statistics of the spatial arrangement of the gray values, is the gray level co-occurrence matrices.

A co-occurrence matrix is a square matrix whose elements correspond to the relative frequency of occurrence of pairs of gray level of pixels separated by a certain distance in a given direction. Formally, the elements of a *GxG* gray level co-occurrence matrix $P_{\mathbf{d}}$ for a displacement vector $\mathbf{d} = (dx,dy)$ is defined as :

$$P_{\mathbf{d}}(i,j) = |\{((r,s),(t,v)) : I(r,s)=i, I(t,v)=j\}| \qquad (11)$$

where $I(\cdot,\cdot)$ denote an image of size NxN with G gray values, $(r,s), (t,v) \in NxN$, $(t,v)=(r+dx, s+dy)$ and $|.|$ is the cardinality of a set.

Haralick, Shanmugan and Dinstein [1] proposed 14 measures of textural features which are derived from the co-occurrence matrices, and each represents certain image properties as coarseness, contrast, homogeneity and texture complexity. Those that are used, in this work, for extracting features in the defect detection of textured images are:

1) *Entropy* :

$$\mathrm{ENT} = -\sum_i \sum_j p(i,j) \log p(i,j) \qquad (12)$$

Entropy gives a measure of complexity of the image. Complex textures tend to have higher entropy.

2) *Contrast* :

$$\text{CON} = \sum_i \sum_j (i-j)^2 p(i,j) \tag{13}$$

Contrast feature is a measure of the image contrast or the amount of local variations present in an image.

3) *Angular Second Moment* :

$$\text{ASM} = \sum_i \sum_j \{p(i,j)\}^2 \tag{14}$$

Angular second moment is a measure of the homogeneity of an image. Hence it is a suitable measure for detection of disorders in textures. For homogeneous textures value of angular second moment turns out to be small compared to non-homogeneous ones.

4)*Inverse Difference Moment* :

$$\text{IDM} = \sum_i \sum_j \frac{1}{1+(i-j)^2} p(i,j) \tag{15}$$

In Eqs. (12) - (15), $p(i,j)$ refers to the normalized entry of the co-occurrence matrices. That is $p(i,j) = P_{\mathbf{d}}(i,j)/R$ where R is the total number of pixel pairs (i,j). For a displacement vector $\mathbf{d} = (dx,dy)$ and image of size NxM R is given by $(N-dx)(M-dy)$.

3. Texture Defect Detection

3.1. General Overview

Texture defect detection can be defined as the process of determining the location and/or extend of various defects using textural properties of the given image. In classification and identification problems, features are derived from local windows. A single class is associated with each window so the feature space tends to form clusters. However, in defect detection problem, due

to the nature of the problem, the features derived from the defective sub-windows, do not cluster but they rather split around or even form clusters within the feature space of non-defective windows, depending on the type and size of the defect. This makes defect detection a complicated and a difficult problem compared to identification and classification.

Any machine vision system, whether it attempts to accomplish recognition, or identification, segmentation or classification tasks, very generally, can be thought to consist of two blocks. The first block is the so-called feature extraction part. This is the place where data is transformed from a higher dimensional space into a lower dimensional form suitable for subsequent processing. Feature extraction is the most important part since the overall performance of a system primarily depends on the performance of this section. The second part involves some kind of decision based on the data obtained in feature extraction phase. In recognition and identification, this is the block that makes matching against data gathered in advance and generates a decision whether the object under concern is among those known a priori. In classification, the decision generated involves grouping of data into classes under certain similarity measure.

It is clear from the decomposed textile images (decomposed by the wavelet transformation) that these images have lowpass characteristic. It is observed that the energy content of the low-low band is around 60 per cent while high-high band has only the 5 percent of the total energy. It is also observed that co-occurrence features compared with wavelet transform features are more powerful in capturing defects [21].

These two observations have motivated the authors to consider extracting co-occurrence features from sub-band images. Advantage of such an approach will be twofold: First, dealing with smaller images would mean improvement in the computational efficiency since the computational complexity of co-occurrence matrices increases as the size of the image increases. Second, disregarding higher frequency bands which most of the time have a noise-like appearance and focusing on the lower resolution images will enhance the defects relative to the background texture.

Thus, using sub-band domain features (as it is called here) have increased the detection rates compared to the features derived from SDCM.

The proposed defect detection system consists of two stages [21]: (i) The feature extraction part first utilizes WT to decompose textured images into sub-bands and then extracts co-occurrence features from the sub-bands and (ii) the detection part, a Mahalanobis-distance classifier that is trained by defect-free samples.

In the following sections, the two blocks that make up the proposed defect detection scheme will be elaborated. In this work, innovations are brought about mainly for the feature extraction part.

3.1. Feature Extraction Part

Given an image $I(n,m)$ of size 2Nx2N, the following steps are applied to extract sub-band domain features:

i- Decompose the image $I(n,m)$ into four bands using wavelet filter coefficients to obtain images I_{LL}, I_{LH} , I_{HL} and I_{HH} where L and H represent lowpass and highpass bands, respectively (Fig. 3).

ii- Calculate energy e_x of each decomposed image as:

$$e_x = \frac{1}{N^2} \sum_n \sum_m \left| I_x(n,m) \right|$$

where x denotes LL, LH, HL and HH bands.

iii- If energy of a sub-band in the decomposed image is significantly lower than the maximum sub-band energy, discard this band and consider only the remaining sub-bands. That is, consider bands with $e_x > Ce_{max}$ where C is a constant less than one.

iv- Divide each sub-band image into non-overlapping sub-windows $S_{x,i}$ of size pxp. Indices x and i denote sub-band and sub-windows, respectively ($1 \le i \le M \; ; \; M = (N/p)^2$). Sub-window of this size in the sub-band image corresponds to a sub-window S_i of size 2px2p in the original image.

v- Derive the co-occurrence matrices P_θ for d =1 (pixel separation distance) and angles θ = (0, π/4, π/2, 3π/4) radians.

vi- Calculate ENT, CON, ASM, IDM for each co-occurrence matrix as in Eqs. (12)-(15).

vii- Compute mean μ_X and standard deviation σ_X for each feature of four angles.

viii- Construct the vector

$$\mathbf{f}_{x,i} = [\mu_{ENT} \ \sigma_{ENT} \ \mu_{CON} \ \sigma_{CON} \ \mu_{ASM} \ \sigma_{ASM} \ \mu_{IDM} \ \sigma_{IDM}].$$

ix- Repeat steps (v) to (viii) for all bands (x) being retained according to the argument in step (iii) .

x- Feature vector for i-th sub-window S_i in the original image is constructed as :

$$\mathbf{s}_i = [\ \mathbf{f}_{LL,i}\ \mathbf{f}_{LH,i}\ ....]^T$$

xi- Repeat steps (v) to (x) for all i.

Since the resolution of the images change when sub-band decomposition is carried out, the defect-free images have also been decomposed into sub-bands for the calculation of the correct classification rates (CR) so that the location of the defects would correspond to those in the ground truth as found by a human expert.

3.3. Detection Part

The detection part of the system is a classifier utilizing Mahalanobis distance measure to assign each feature vector (i.e., each sub-window of the image) a label (class) as defective or non-defective. Formally, the classification consists of a learning phase and a classification phase. These phases will be elaborated in the subsequent sections.

Learning phase

(i) Given *k* defect-free 2Nx2N fabric images, calculate the feature vectors for each sub-window of the image using the feature extraction scheme given above. Consider these vectors as the true feature vectors and name them as $\mathbf{t}_i$ ($1 \le i \le Mk$).

(ii) Compute the mean vector **m** and the covariance matrix **K** for the feature vectors $\mathbf{t}_i$.

Classification phase

(i) Given a test image calculate the feature vectors $\mathbf{s}_i$'s using the feature extraction scheme given above.

(ii) Compute the Mahalanobis distance d_i between each feature vector $\mathbf{s}_i$ and the mean vector **m**

$$d_i = (\mathbf{s}_i - \mathbf{m})^T \mathbf{K}^{-1} (\mathbf{s}_i - \mathbf{m}) \qquad (16)$$

where **K** is the covariance matrix. Vector **m** and matrix **K** are determined in the learning phase.

(iii) Classify a sub-window S_i for which d_i exceeds a threshold value α as defective, else identify it as non-defective. i.e.,

$$S_i = \begin{cases} \text{defective} & \text{if} \quad d_i > \alpha \\ \text{nondefective} & \text{otherwise} \end{cases}$$

The threshold value α is determined by the formula

$$\alpha = D_m + \eta (D_q - D_m) \qquad (17)$$

D_m and D_q are, respectively, the sample median and the sample upper quartile of the order statistics D_i obtained when distances d_i arranged in ascending order and η is a constant determined experimentally. So, the second term of summation in Eq. (17) is the confidence interval. For a 2Nx2N sized image partitioned into M sub-windows of size 2px2p, $D_m = (D_{M/2} + D_{M/2+1})/2$ and $D_q = (D_{M-M/4} + D_{M-M/4+1})/2$. In calculating the threshold, for an image, the sample median of the distances of sub-windows from the learned sample in place of mean is used since if there are defective sub-windows, the mean will not be a reliable measure.

Intuitively, what the classifier does is to assign the image sub-windows with considerable difference from the rest as defective.

4. Implementation And Results

One possible application domain for the texture defect detection algorithms, among many others, is the textile fabric inspection. Hence, for the experimental justification of the algorithm, real fabric images acquired by a CCD camera in a laboratory environment are used [21]. The database consists of 36 256x256 sized 8-bit long gray level images. Seventeen of those images are void of defects while each of the remaining 19 contains defects of different size (extended-localized) and nature (point-line) that occur most frequently in the textile fabric production process (Fig. 4). Training of the system is attained by using16 defect free images. The rest of the set has been used for testing the algorithm. Decomposition of raw images into sub-bands is performed using Battle-Lemarie wavelet filter coefficients and the length of the decomposition filter has been chosen as 16. Before computing the co-occurrence matrices, sub-band images are quantized into 8-levels (3 bits). This results in enormous computational saving while extracting the (ENT, CON, ASM and IDM) features, without any significant effect on the final results. Window size used, in scanning the images depends both on the resolution of the camera used for image acquisition and the textural properties of the fabrics as well as how localized the defects. In the experiments, the highest performance (90.78%) is obtained by using 32x32 sized non-overlapping sub-windows for the original image. This performance can be slightly improved, at the expense of the computation time, by introducing some sort of overlap between the sub-windows for better treatment of thin line defects occurring at the border of the adjacent cells. In the experiments, the value of constant C in step (iii) of the feature extraction algorithm is chosen as 0.35. For this value, only the LL band is retained. When the tests are repeated for smaller values of C such that all four bands are considered, the results have not changed considerably. Figure 5 illustrates the performance of SBCM method when only the LL band or all four bands are retained. Results indicate that using only the lower resolution images is sufficient. This indicates that C equals 0.35 is a good choice.

For comparison purposes, the SDCM method [1], the MRF based method [15], PSWT [7], wavelet packet signature (WPS)[8,16] and Gabor filtering[24,25] are implemented for the available database.

For the SDCM method, after quantizing the image to 8 levels and dividing it to 32x32 non-overlapping sub-windows, the co-occurrence matrices P_θ are derived. The co-occurrence matrices are computed for d =1 (pixel separation distance) and angles θ = (0, π/4, π/2, 3π/4) radians. Then the same Haralick features, namely, ENT, CON, ASM, IDM for each co-occurrence matrix are calculated. Then the feature vectors are constructed using the mean μ_X and the standard deviation σ_X for each feature of four. To extract features for the MRF, the method discussed in [15] is used. A feature vector of length 25 computed from the sufficient statistics of a ninth order MRF model is formed for each sub-windows of size 32x32. For the PSWT method, the image is again divided into non-overlapping sub-windows of size 32x32 and each sub-windows is decomposed into sub-band images by 2-level pyramid structured wavelet transform. For each decomposed sub-band image (children node), the energy is calculated. The feature vector of each sub-window consists of the energies of the 7 sub-band images.

For the WPS, 2-level wavelet packet expansion is applied to each sub-window of size 32x32. The feature vector of each sub-window consists of the energy values of the 1-level and 2-level decomposed sub-band images. Specifically, the feature vectors consist of 20 different energy values.

The textured images are decomposed using 28 complex 2-D Gabor filter tuned at seven radial frequencies (F) each one octave apart ($1\sqrt{2}$, $2\sqrt{2}$, $4\sqrt{2}$, $8\sqrt{2}$, $16\sqrt{2}$, $32\sqrt{2}$, $64\sqrt{2}$ cycles/image-width) and four orientations (0, 45, 90 and 135 degrees). Orientation bandwidth (Ω) is chosen to be 45 degrees. These 28 filters form a nearly orthogonal set and provide uniform coverage of the frequency plane [24]. The output image of each filter is divided into 32x32 sized

non-overlapping sub-windows and the energy of each sub-window is calculated. Thus, the feature vector of each sub-window consists of 28 energy values.

For completeness, the sub-band domain MRF (SBMRF) method is also implemented. In this method, the MRF models of the sub-band images, rather than the raw images, are obtained by wavelet transformation. For SBMRF, on the other hand, 16x16 sub-windows are used to extract ninth order MRF features from low-low band images obtained by decomposition of the original 256x256 sized fabrics into four bands using Battle-Lemarie filters.

In Fig.6, the correct detection versus false alarm rates, known as receiver operating curve for all methods are plotted. The classification rates for all set of features are depicted in Fig.7. The classification rate, CR, is defined as:

$$CR=100* (N_{cc}+ N_{dd})/ N_{total} \quad (18)$$

where N_{cc} , N_{dd} and N_{total} are, respectively, the number of sub-windows being classified as clean when they are clean, the number of sub-windows being classified as defective when they are defective and the total number of sub-windows being tested. Results, as depicted in Figs.6-7, demonstrate clearly the advantage of the proposed algorithm that incorporates some sort of frequency information on the features by the use of sub-band decomposition scheme. In order to show the power of SBCM features over the SDCM, the distance values of the sub-windows for the defective fabric illustrated in Fig. 4(q) are plotted in Fig.9. It is very interesting to notice how the defective cells have been enhanced with respect to the clean ones in the SBCM method [22]. Computational requirements of each method are summarized in Table 1.

In a sense features derived using two approaches to texture modeling, namely, statistical (SDCM) and signal processing (PSWT, WPS, Gabor) and a hybrid of both (SBCM) are compared in terms of defect detection.

The following conclusions can be derived when the proposed method is compared with the signal processing methods; In terms of false alarm and correct detection rates it is ranked

immediately after the Gabor filtering method (Fig.6). The sole disadvantage may be the selection of feature set in case of textures with very different characteristics. It is known that multi-channel Gabor filters are optimum in terms of spatial/spatial-frequency localization. Detection capacity of multi-frequency energy features derived from Gabor filtered images is apparent in the SOC curves (Fig.6). In the experiments carried out, most of the defects are detected with relatively small false alarm rates. However, when computational and storage requirements are concerned one can not speak about the same optimality. The computational demand is approximately as much as 100 times that of wavelet transform based method. A possible remedy is to reduce the filter set by incorporating feature selection or parameter tuning algorithm as suggested in [24] and [25]. But even if a single filter is used, the computational requirement can not be less than that of WPS based system. In the experiments 28 filters are used. When different subsets from these 28 filters were selected, the detection rates dropped considerably. The proposed method is superior than the two wavelet based methods, namely, pyramid structured wavelet transform and the wavelet packet signatures which perform almost the same. Computationally, SBCM method is superior to the PSWT, WPS and Gabor filters.

Comparing the proposed method with MRF, it is observed that performance-wise they are almost at the same level while the computational saving introduced by SBCM method is around 43% (Fig.5-6 and Table I).

Comparing the proposed method with SDCM, it is observed that SBDM performs better in terms of detection at an increase of 50% computational complexity.

When the MRF and the SBMRF methods are compared, the sub-band domain model introduces an increase of 1% in classification rate.

In general it can be stated that the method that is applied to the sub-band images is superior over the method applied to the raw images (i.e. SBCM is superior to SDCM, SBCM is superior to WPS and PSWT, SBMRF is superior to MRF).

SOC curves and classification rates about all methods are plotted in the Figs. 6 and 7, respectively. Computational requirements of each method are summarized in Table I.

5. Conclusions

In this paper, an efficient texture defect detection method based on SBCM features is introduced. When textures with frequency content mostly concentrated on a single band are considered, focusing on that particular band and discarding the others, which carry information with low discriminatory power, improves the detection performance. In general, it can be stated that the method that is applied to the sub-band images is superior than the same method applied to the raw images (i.e. SBCM is superior to SDCM, SBCM is superior to WPS and PSWT, SBMRF is superior to MRF). Considering the results obtained with respect to computational complexity and reliability, the SBCM approach seems to be feasible for real-time factory implementations.

Acknowledgements

We would also like to thank Altınyıldız A.Ş. for providing the defective fabrics.

References

[1] R.M. Haralick, K. Shanmugan and Its'Hak Dinstein, "Textural Features for Image Classification", *IEEE Trans. on SMC*, 3 (1973) 610-621.

[2] L.H. Siew, R.M. Hodgson and E.J. Wood, "Texture Measures for Carpet Wear Assessment", *IEEE Trans. on PAMI*, 10 (1988).

[3] J.S. Weszka, C.R. Dyer and A.Rosenfeld, "A Comparative Study of Texture Measures for Terrain Classification", *IEEE Trans. on SMC*, 6 (1976) 269-285.

[4] I. Daubechies, "Orthonormal Bases of Compactly Supported Wavelets", *Comm. on Pure and App. Mathematics*, 41 (1988) 909-996.

[5] S. G. Mallat, "A Theory for Multiresolution Signal Decomposition: The Wavelet Representation", *IEEE Trans. on PAMI*, 11 (1989) 674-693.

[6] A.C. Bovik, M.Clark and W.S. Geisler, "Multichannel Texture Analysis Using Localized Spatial Filter", *IEEE Trans. on PAMI*, 12 (1990) 55-73.

[7] T. Chang and C.-C.Jay Kuo, "Texture Analysis and Classification with Tree-Structured Wavelet Transform", *IEEE Trans. on IP*, 2 (1993) 429-441.

[8] A. Laine and J. Fan, " Texture Classification by Wavelet Packet Signatures", *IEEE Trans. on PAMI*, 15 (1993) 1186-1191.

[9] P.P.Ohanian and R.C.Dubes, "Performance Evaluation for Four Classes of Textural Features", *Pattern Recognition*, 25 (1992) 819-833.

[10] Erçil, A. and B. Özüyılmaz, Automated Visual Inspection of Metallic Surfaces *The Proc. The Third International Conference on Automation, Robotics and Computer Vision (ICARCV'94),* 2 (1994) 1950-1954.

[11] Jain, A. K., F. Farrokhina and D. Alman, Texture Analysis of Automotive Finishes", *Proc. SME Machine Vision Applications Conference*, 1 (1990) 1-16.

[12] Chen, J. and A. K. Jain, A Structural Approach to Identify Defects on Textural Images, *Proc. IEEE International Conference on Systems, Man, and Cybernetics,* 1 (1988) 29-32.

[13] Conners, R., "Identifying and Locating Surface Defects in Wood", *IEEE Trans. Pattern Anal. and Mach. Intell*., 5(6) (1983).

[14] Dewaele, P., L. Van Gool, A. Oosterlinchk, "Texture Inspection with Self-Adaptive Convolution Filters", *Proc. 9th International Conference on Pattern Recognition,* 1 (1988) 14-17.

[15] F.S. Cohen, Z. Fan, and S. Attali, "Automated Inspection of Textile Fabrics Using Textural Models", *IEEE Trans. on PAMI*, 13 (1991) 803-808.

[16] C.S Lee, C.-H. Choi, J.Y. Choi, Y.K. Kim and S.H. Choi, "Feature Extraction Algorithm Based on Adaptive Wavelet Packet for Surface Defect Classification", *IEEE Int. Conf. on Image Proc.*, (1996) 673-675.

[17] W.J. Jasper, S.J. Gernier and H. Potlapalli, "Texture Characterization and Defect Detection Using Adaptive Wavelets", *Optical Engineering,* 35(11) (1996) 3140-3149.

[18] K.Y. Song, J. Kittler and M. Petrou, "Defect Detection in Random Color Textures", *Image and Vision Computing*, 14(9) (1996) 667-683.

[19] C. Ciamberlini, F. Francini, G. Longobardi, P. Sansoni, " Defect Detection in Textured Materials with Structured Detectors and Self Adaptable Masks", *Optical Engineering,* 35(3) (1996) 838-844.

[20] J.G: Campbell and f. Murtagh, " Automatic Visual Inspection of Woven Textiles Using a 2-D Stage Defect Detector", *Optical Engineering,* 37(9) (1998) 2536-2542.

[21] A. Latif Amet, ''Texture Defect Detection Using Wavelet Transforms'', M.S. Thesis, Boğaziçi University, Istanbul, Turkey, (1997).

[22] Akansu, A. N. and R. A. Haddad, *Multiresolution Signal Decomposition*, Academic Press Inc., Boston, (1992).

[23] Mallat, S., "Multifrequency Channel Decomposition of Images and Wavelet Models," *IEEE Transactions on Acoustics, Speech, and Signal Processing*, 37(12) (1989) 2091-2110.

[24] Jain, A.K. and F. Farrokhnia, "Unsupervised Texture Segmentation Using Gabor Filters," *Pattern Recognition*, 24(2) (1991) 1167-1186.

[25] Teuner, A., O. Pichler and B. J. Hosticka, "Unsupervised Texture Segmentation of Images Using Tuned Matched Gabor Filters," *IEEE Transactions on Image Processing*, 4(6) (1995) 863-870.

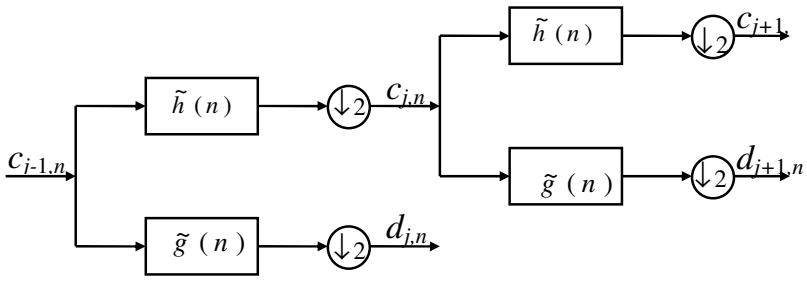

Figure 1 Two-level pyramid structure wavelet decomposition scheme

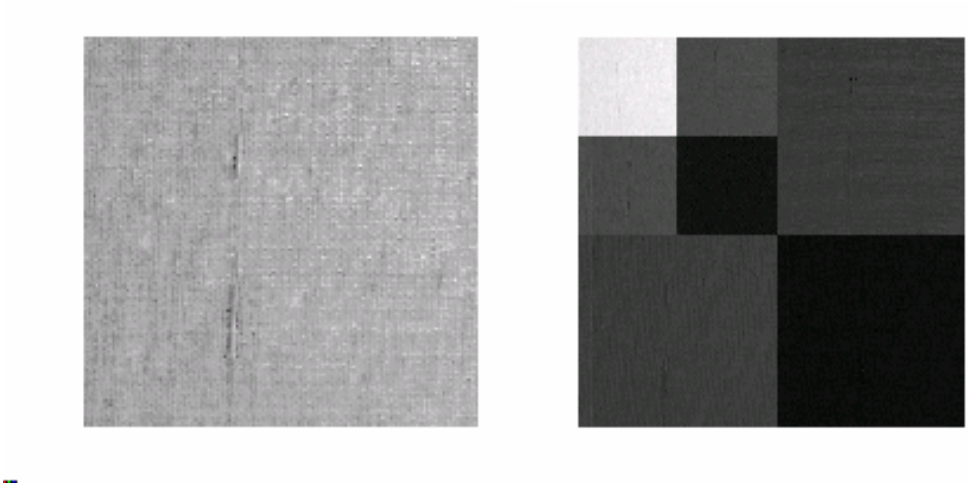

(a) **(b)**

Figure 2 (a) A textile fabric image, (b) its wavelet transform

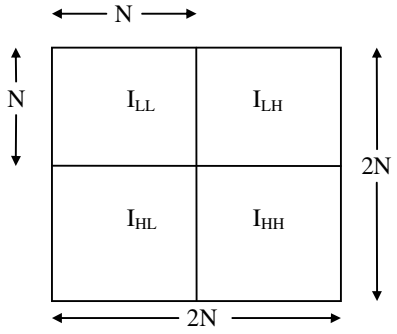

Figure 3 Decomposition of image I(n,m)

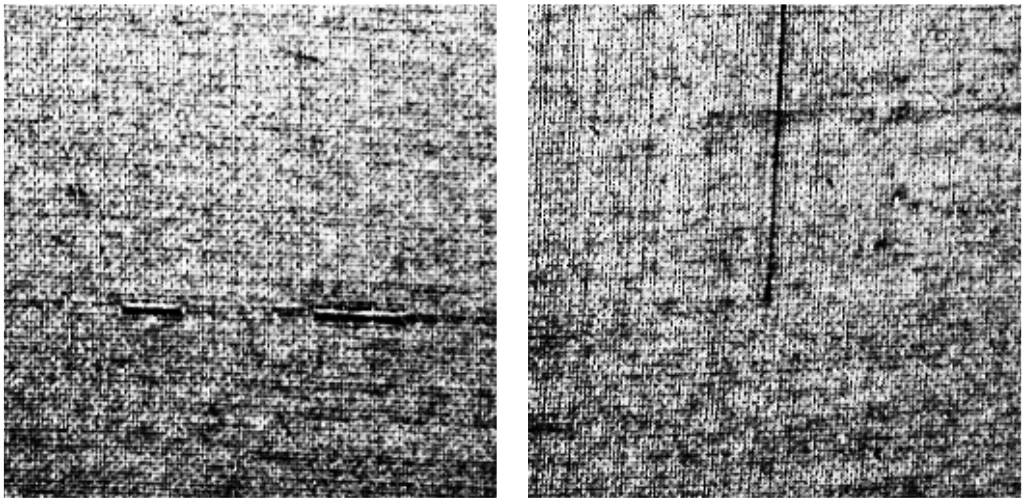

(a) **(b)**

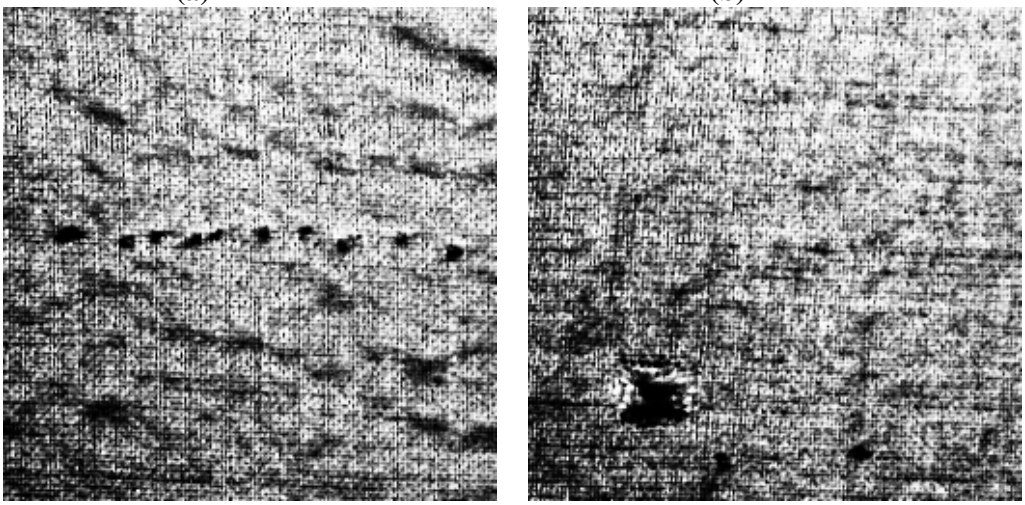

(c) **(d)**

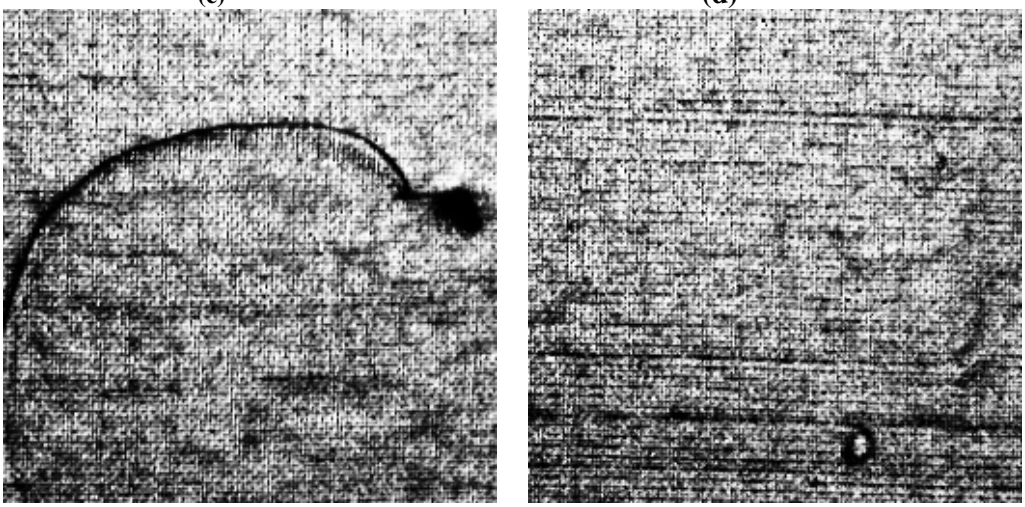

(e) **(f)**

Figure 4 (cont.)

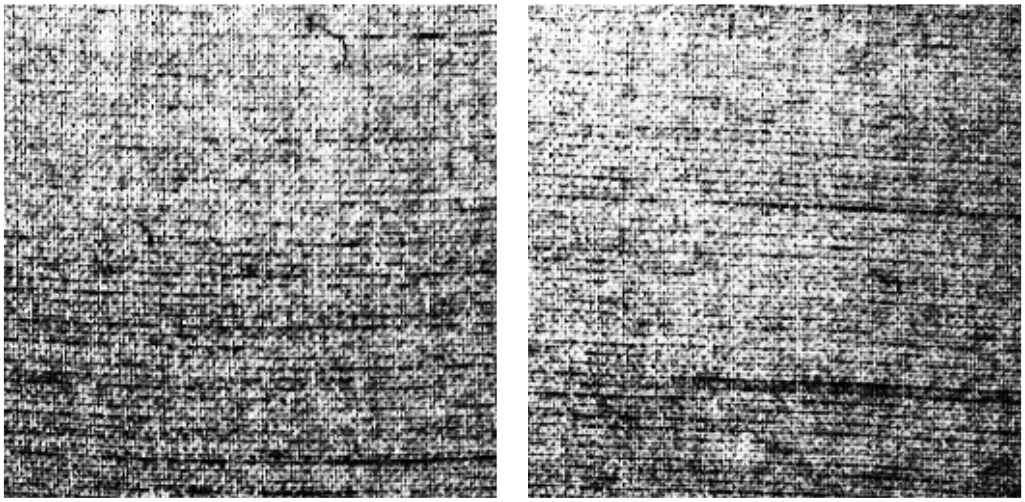

(g) **(h)**

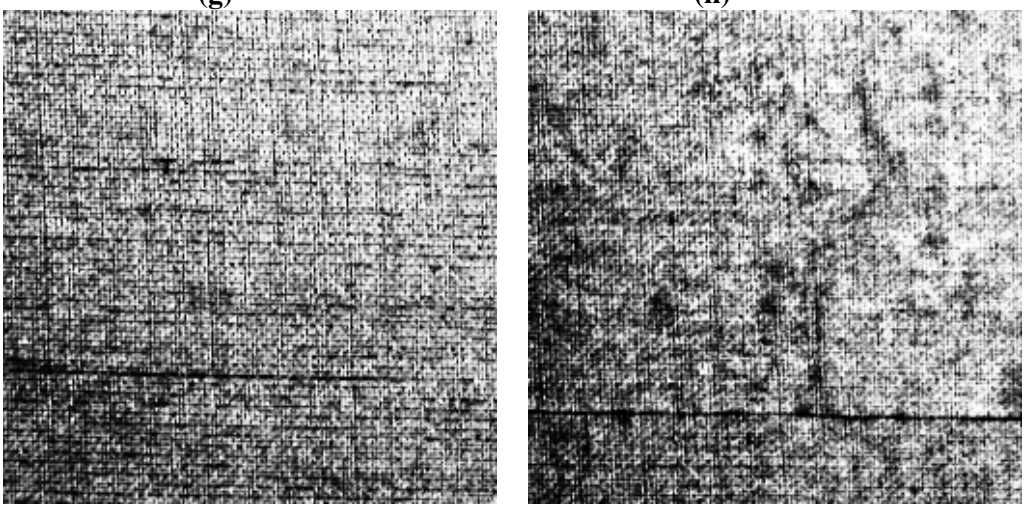

(i) **(j)**

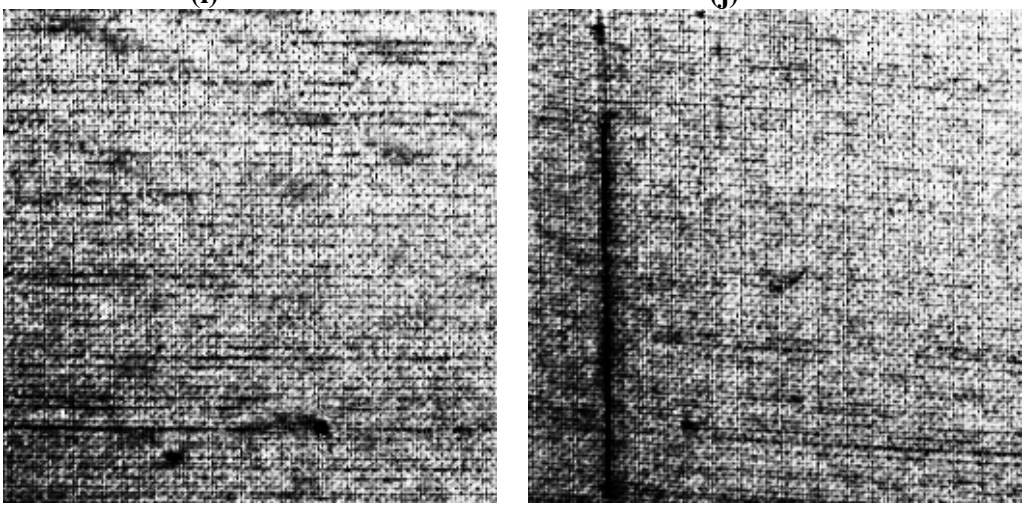

(k) **(l)**

Figure 4 (cont.)

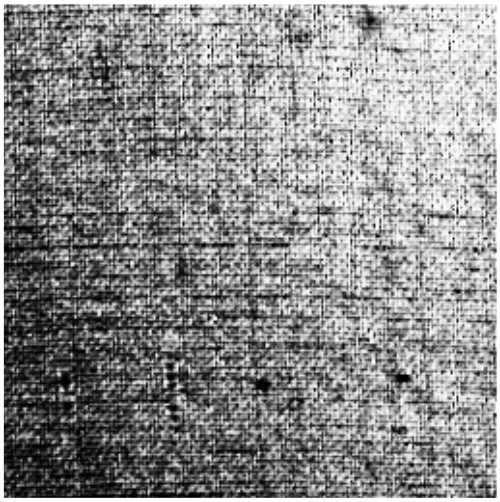

(m)

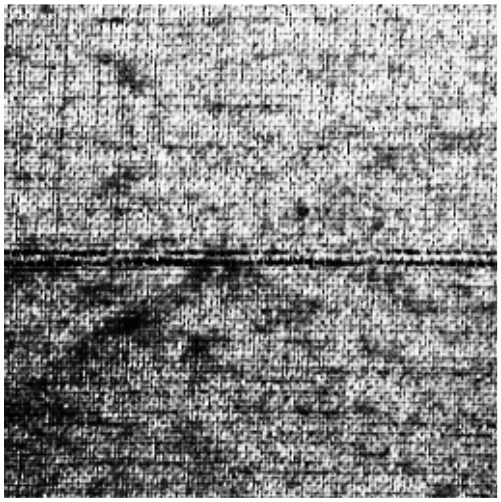

(n)

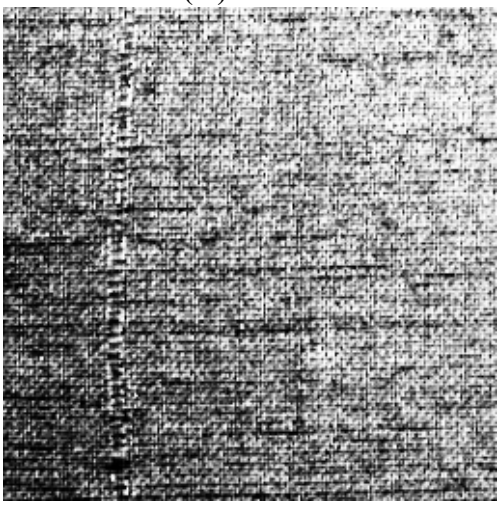

(o)

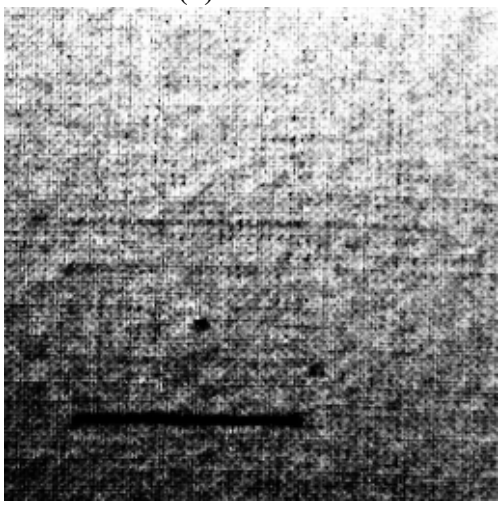

(p)

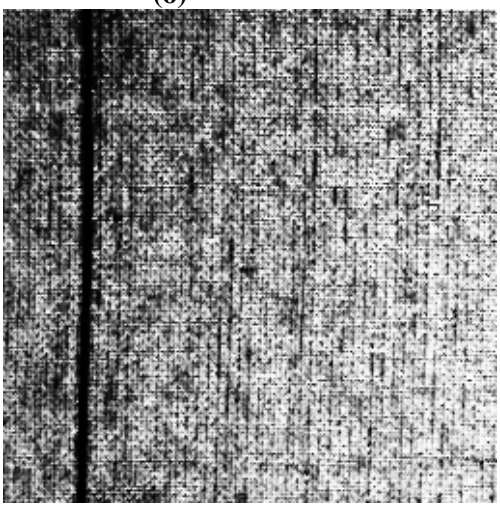

(q)

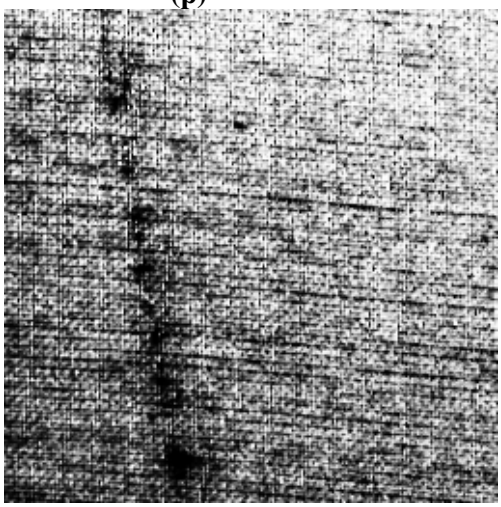

(r)

Figure 4 (cont.)

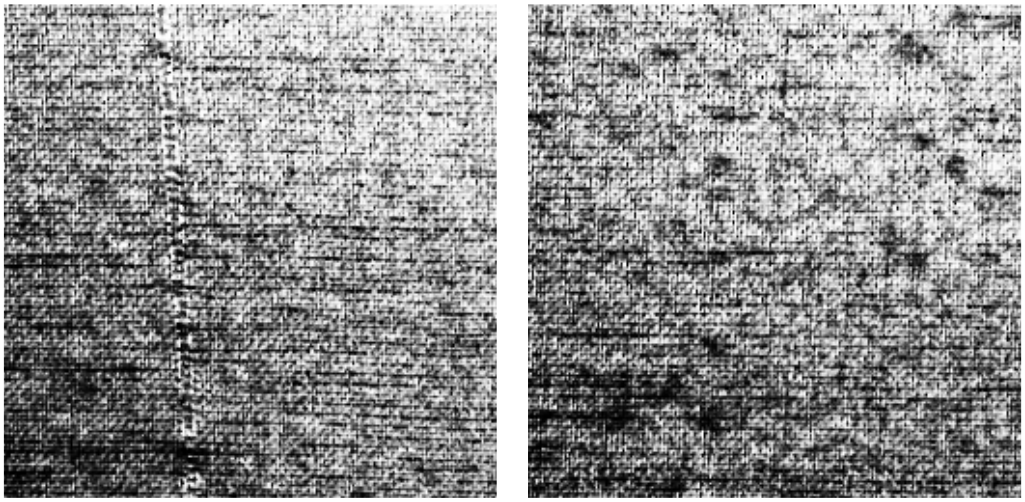

(s) **(t)**

Figure 4 (a)- (s) Defective textile images
(t) Nondefective (clean) textile image

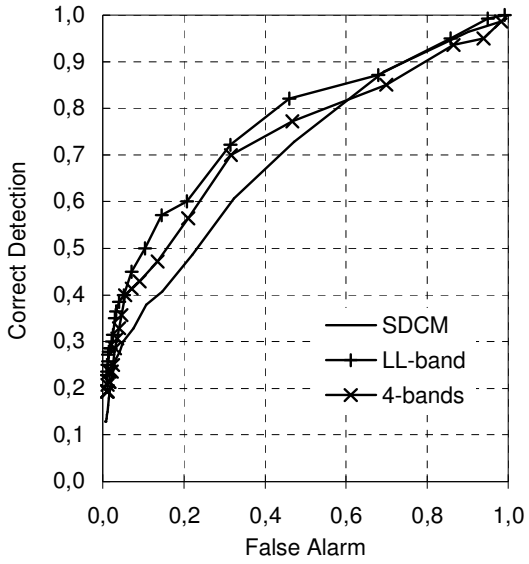

Figure 5 Average SOC curves for SDCM and SBCM based systems

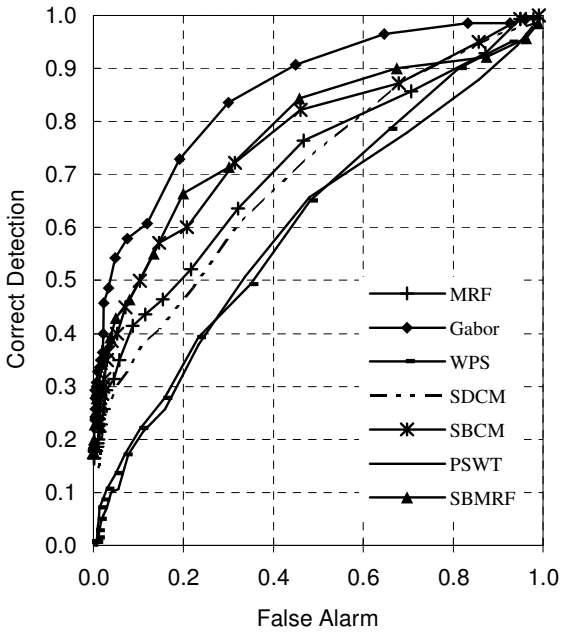

Figure 6 Average SOC curves for all methods

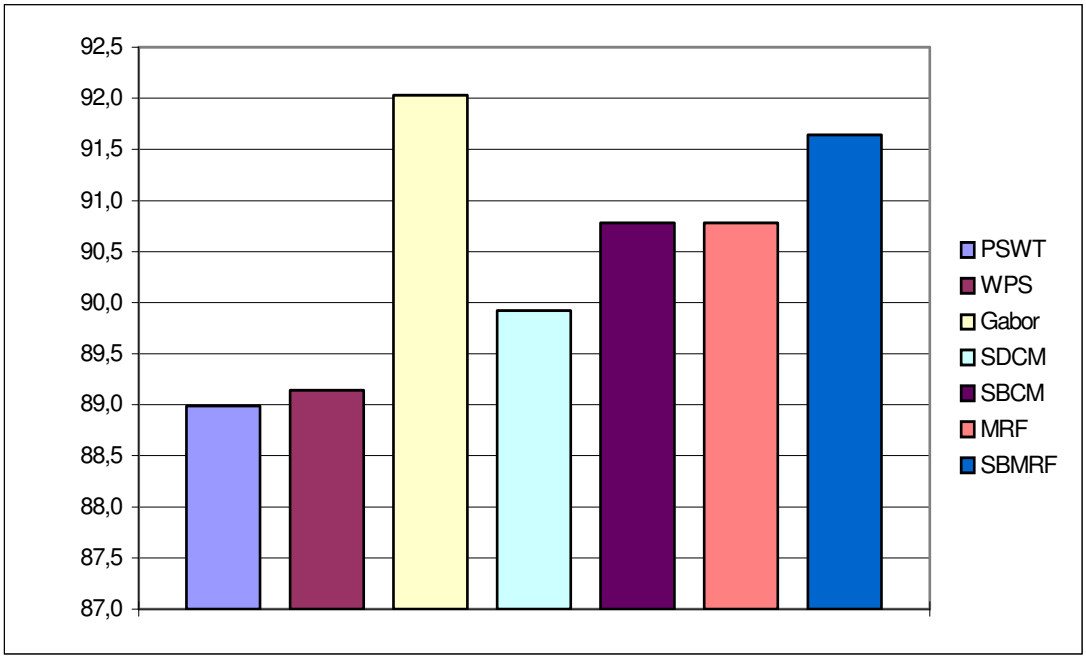

Figure 7 Performance of each method in terms of classification rates

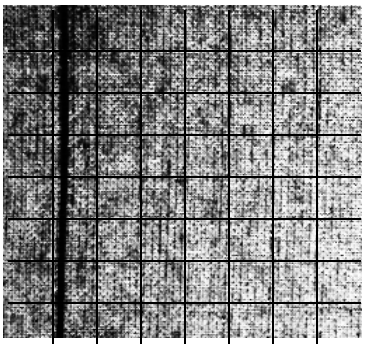

Figure 8 Defective fabric image illustrated in figure 4(l) partitioned into 32x32 subwindows

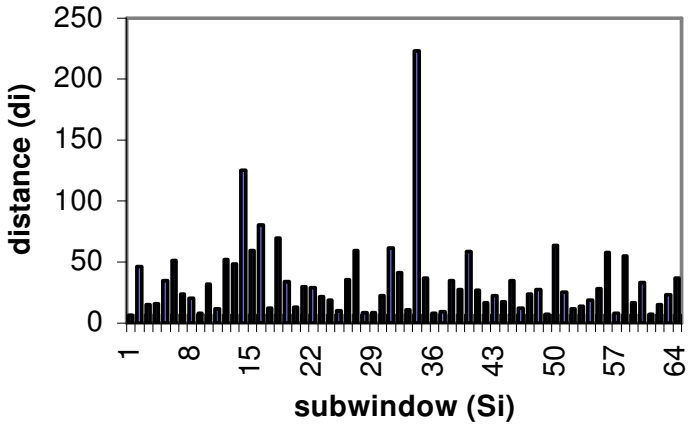

(a)

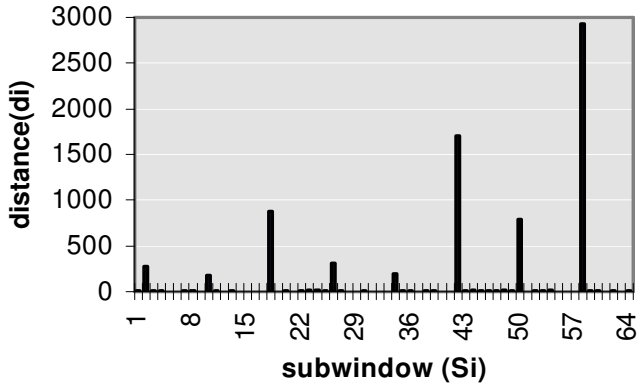

(b)

Figure 9 Distance (d_i) values for the subwindows S_I (S_i :i=1 to 64) of defective image illustrated in figure 4 (q) obtained using **(a)** SDCM and **(b)**SBCM (bottom).